Synthetic dissipation and cascade fluxes in a turbulent quantum gas

Nir Navon[1†], Christoph Eigen[2], Jinyi Zhang[2], Raphael Lopes[2*], Alexander L. Gaunt[2,3], Kazuya Fujimoto[4†], Makoto Tsubota[5], Robert P. Smith[2,6] and Zoran Hadzibabic[2]

[1] Department of Physics, Yale University, New Haven, Connecticut 06520, USA

[2] Cavendish Laboratory, University of Cambridge, J.J. Thomson Avenue, Cambridge CB3 0HE, United Kingdom

[3] Microsoft Research, 21 Station Road, Cambridge CB1 2FB, United Kingdom

[4] Department of Physics, University of Tokyo, 7-3-1 Hongo, Bunkyo-ku, Tokyo 113-0033, Japan

[5] Department of Physics and Nambu Yoichiro Institute of Theoretical and Experimental Physics, Osaka City University, 3-3-138 Sugimoto, Sumiyoshi-Ku, Osaka 558-8585, Japan

[6] Clarendon Laboratory, University of Oxford, Parks Road, Oxford OX1 3PU, United Kingdom

[†]To whom correspondence should be addressed;
E-mail: nir.navon@yale.edu, fujimoto@cat.phys.s.u-tokyo.ac.jp

Scale-invariant fluxes are the defining property of turbulent cascades, but their direct measurement is a notorious problem. Here we perform such a measurement for a direct energy cascade in a turbulent quantum gas. Using a time-periodic force, we inject energy at a large lengthscale and generate a cascade in a uniformly-trapped three-dimensional Bose gas. The adjustable trap depth provides a high-momentum cutoff k_{D}, which realizes a synthetic dissipation scale. This gives us direct access to the particle flux across a momentum

[*]Present address: Laboratoire Kastler Brossel, Collège de France, CNRS, ENS-PSL University, UPMC-Sorbonne Université, 11 Place Marcelin Berthelot, F-75005 Paris, France

shell of radius k_{D}, and the tunability of k_{D} allows for a clear demonstration of the zeroth law of turbulence: we observe that for fixed forcing the particle flux vanishes as k_{D}^{-2} in the dissipationless limit $k_{\mathrm{D}} \to \infty$, while the energy flux is independent of k_{D}. Moreover, our time-resolved measurements give unique access to the pre-steady-state dynamics, when the cascade front propagates in momentum space.

The discovery in 1941 by Kolmogorov and Obukhov of a universal law describing the transfer of energy from large to small lengthscales in turbulent flows was a conceptual breakthrough (*1, 2*). Despite their complex spatiotemporal dynamics, turbulent flows often obey a simple generic picture: the energy injected into the system at a large lengthscale flows locally in Fourier space, through lengthscales in the so-called inertial range where no dissipation occurs, until it is dissipated at some small lengthscale. In Fig. 1A, we depict such turbulent-cascade dynamics for a compressible field in real space. Here, a field initially at rest is at times $t > 0$ continuously forced at a large lengthscale $1/k_{\mathrm{F}}$, and the excitations propagate to smaller lengthscales due to nonlinear interactions. Once the excitations first reach the dissipation scale $1/k_{\mathrm{D}}$, at time t_{d}, the field fluctuates on all lengthscales from $1/k_{\mathrm{F}}$ to $1/k_{\mathrm{D}}$. If a steady state is established within the momentum range k_{F} to k_{D}, from thereon energy is dissipated at k_{D} at the same rate at which it is injected at k_{F}. In such a steady state, the momentum-space distributions of quantities such as the energy or wave amplitude, are generically scale-free power laws.

Many quantitative theoretical predictions about turbulence are based on taking the mathematical limits $k_{\mathrm{F}} \to 0$ and $k_{\mathrm{D}} \to \infty$ (*3*). Such formal treatments lead to predictions that are elegant, but often also counter-intuitive. A key prediction of this kind is that for $k_{\mathrm{D}} \to \infty$ the steady-state cascade corresponds to a scale-invariant (k-independent) energy flux through momentum space, but no particle flux (*4*).

Experimentally, the steady-state power-law spectra of various quantities have been exten-

sively studied (*5–9*), while the equally fundamental cascade fluxes are harder to measure (*10–13*). Recently, ultracold atomic gases have emerged as a novel platform for studies of turbulence (*9, 14–22*), which offers new experimental possibilities. Here, we use an atomic gas to directly measure cascade fluxes in a turbulent system. Moreover, our dissipation scale is tuneable, which allows us to explore how the fluxes depend on $k_{\rm D}$, and to reconcile the experimental observations with the formal predictions for $k_{\rm D} \to \infty$. Our system also allows a time-resolved study of the initial stage of turbulence (*23–25*), when a steady state is not yet established, which reveals how the cascade front propagates in momentum space.

Our experiment starts with a weakly interacting Bose-Einstein condensate of $N \approx 1.2 \times 10^5$ atoms of ^{87}Rb in the uniform potential of a cylindrical optical box trap of radius $R \approx 16$ μm and length $L \approx 27$ μm (see Fig. 1B and (*26*)). At the end of the initial preparation of the gas the non-condensed fraction is < 10 % and the chemical potential is $\mu \approx k_{\rm B} \times 2$ nK, corresponding to a healing length $\xi \approx 1.2$ μm $\ll R, L$. As in (*9*), we initiate a turbulent cascade by injecting energy at the system-size lengthscale, using a spatially uniform force $\mathbf{F}_{\rm s}(\mathbf{r}, t) = F_0 \sin(\omega_{\rm s} t)\hat{\mathbf{x}}$; here $\hat{\mathbf{x}}$ is a unit vector along the box symmetry axis, $F_0 L \approx k_{\rm B} \times 2.5$ nK, and $\omega_{\rm s} \approx 2\pi \times 9$ Hz is tuned to resonantly excite the sound wave of wavelength $2L$ (so $k_{\rm F} = \pi/L$) (*27*). This large-scale, anisotropic forcing is represented in Fig. 1C as a small dark blue area elongated along k_x. After several seconds of shaking, in the inertial range our gas has a time-invariant, statistically isotropic momentum distribution, $\langle n(\mathbf{k}) \rangle \approx n(k) \propto k^{-\gamma}$, with $\gamma \approx 3.5$ (*9, 28*). This time invariance implies that the energy and particle fluxes through this k-range are k-independent, but it does not reveal their values. Here we extract the cascade fluxes by studying the dissipation in our gas.

In conventional fluids one observes macroscopic (hydrodynamic) degrees of freedom and the dissipation occurs in the form of heating, *i.e.* transfer of energy into the microscopic degrees of freedom. This dissipation is set by the viscosity ν, which is generally not tuneable. Moreover,

the resulting minute heating is often difficult to measure, due to thermal coupling of the fluid with its surroundings (*30*). Our system is thermally isolated from the environment and we have direct access to all the microscopic degrees of freedom, so the dissipation occurs only in the form of (readily measurable) particle loss. The optical box (Fig. 1B) has a non-infinite energy depth U_{D}, so particles with a sufficiently large energy leave the box; in momentum space U_{D} corresponds to a sphere of radius $k_{\mathrm{D}} = \sqrt{2mU_{\mathrm{D}}}/\hbar$ (Fig. 1C), where m is the atom mass. This simple feature realizes a synthetic dissipation scale, with U_{D} defining the particle and energy sink. Crucially, this dissipation scale can be tuned by changing the trapping laser power (*31*).

Formally, within the assumptions of the wave-turbulence theory, from the equations of motion one can derive a continuity equation with a source and a sink, that is local in momentum space (*3*):

$$\frac{\partial n(\mathbf{k},t)}{\partial t} = F(\mathbf{k},t) - D(\mathbf{k},t) - \nabla_{\mathbf{k}} \cdot \mathbf{\Pi}_n(\mathbf{k},t)\,. \tag{1}$$

Here $F(\mathbf{k},t)$ describes the forcing, $D(\mathbf{k},t)$ the dissipation, and $\nabla_{\mathbf{k}} \cdot \mathbf{\Pi}_n$ the nonlinear interactions, where $\mathbf{\Pi}_n$ is the particle flux. For $F = D = 0$, the steady-state solutions are zero-flux equilibrium thermodynamic states. If F and D are nonzero but are localized in k space, one can also get non-equilibrium steady-state solutions with a nonzero scale-independent flux sustained by the source F and the sink D.

For an isotropic outflow, the total radial particle flux is $\Pi_n(k) = 4\pi k^2 |\mathbf{\Pi}_n(\mathbf{k})|$. Hence, from Eq. (1), in the inertial range $4\pi k^2\, \partial n/\partial t = -\partial \Pi_n/\partial k$. Integrating over k yields the intuitive result that we can measure the particle flux through the shell at k_{D} by simply counting the atoms remaining in the trap (see Fig. 1C):

$$\frac{\partial N}{\partial t} \equiv -\Pi_n(k_{\mathrm{D}},t)\,, \tag{2}$$

and for a (non-equilibrium) steady state, with time-invariant $n(k)$ in the inertial range (*9*), the particle flux is k- and t-independent (*32*), so $\Pi_n(k_{\mathrm{D}},t) = \Pi_n(k,t) = \Pi_n$.

In steady state, the total radial energy flux, $\Pi_{\mathcal{E}}(k,t)$, is also k- and t-independent in the inertial range, and is equal to the rate of energy dissipation. To relate it to Π_n, we consider the pertinent case of weakly-interacting particles with a dispersion relation $\omega(k)$, so the energy spectrum is $\mathcal{E}(k,t) = \hbar\omega(k)n(k,t)$ (in our case $\omega(k) \propto k^2$). At $k < k_{\rm D}$ microscopic interactions drive particles to both smaller and higher k, so the relationship between the *net* energy and particle fluxes, $\Pi_{\mathcal{E}}$ and Π_n, is nontrivial; one might naively expect that $\Pi_{\mathcal{E}}(k) = \hbar\omega(k)\,\Pi_n(k)$, but this cannot be true if both $\Pi_{\mathcal{E}}$ and Π_n are k-independent, while $\omega(k)$ is not. However, at $k_{\rm D}$ the particles flow only one way, since there is no 'back-flow' from the sink into the inertial range, so one can intuitively write

$$\Pi_{\mathcal{E}}(k_{\rm D}) = \hbar\omega(k_{\rm D})\,\Pi_n(k_{\rm D})\,. \tag{3}$$

Steady state then requires $\Pi_{\mathcal{E}} = \hbar\omega(k_{\rm D})\,\Pi_n$ at all k in the inertial range; for our $\omega(k)$ this means that $\Pi_{\mathcal{E}} \propto k_{\rm D}^2\,\Pi_n$. Note that to formally derive Eq. (3) one multiplies Eq. (1) by $\hbar\omega(k)$ and invokes the continuity equation for the energy to get

$$\frac{\partial\Pi_{\mathcal{E}}(k,t)}{\partial k} = \hbar\omega(k)\frac{\partial\Pi_n(k,t)}{\partial k} \tag{4}$$

in the inertial range. For $k < k_{\rm D}$ this equation is trivially satisfied by both of its sides being zero, and does not impose any relation between $\Pi_{\mathcal{E}}(k)$ and $\Pi_n(k)$. However, integrating it across a shell around $k_{\rm D}$, and setting $n(k)$ and all fluxes to zero for $k > k_{\rm D}$, recovers Eq. (3).

Experimentally, we vary $k_{\rm D}$, while keeping F_0 fixed, and measure $\Pi_n(k_{\rm D})$ as per Eq. (2). To mitigate the effects of the long-term few-percent drifts in the initial N, and of the additional atom loss through collisions with the background-gas particles, we perform differential measurements of the cascade-induced atom loss, $N_{\rm loss}$, with reference measurements taken by setting F_0 to zero in an otherwise identical experimental sequence.

In Fig. 2, we show $N_{\rm loss}$ as a function of the shaking time $t_{\rm s}$, for various values of $U_{\rm D}$. In all cases at short times we observe no loss (within errors). This is consistent with the expectations

that no losses occur at $k < k_{\rm D} \propto \sqrt{U_{\rm D}}$ and that initially it takes time for the excitations to cascade to $k_{\rm D}$, when a steady state can be established (see Fig. 1). For $t_{\rm s}$ longer than some onset time, $t_{\rm d}$, the loss rate $\partial N_{\rm loss}/\partial t$ is essentially constant in time, as long as the total loss is relatively small ($< 30\%$ of the initial $N \approx 1.2 \times 10^5$). The dashed lines show piece-wise linear fits that we use to extract, for each $U_{\rm D}$, both $t_{\rm d}$ and the subsequent initial loss rate, which we identify with the steady-state particle flux $\Pi_n = \Pi_n(k_{\rm D})$. At much longer times, $t_{\rm s} \gg t_{\rm d}$, the steady-state assumption can no longer hold, because the losses significantly deplete the low-k source of atoms.

In Fig. 3, we show a log-log plot of Π_n versus $U_{\rm D}$ (*31*). We observe power-law behavior $\Pi_n \propto U_{\rm D}^{-1.05(8)} \propto k_{\rm D}^{-2.10(16)}$. We complement these measurements with numerical simulations based on the Gross-Pitaevskii equation, for the same forcing protocol and without any free parameters (see (*27*) for details). The numerical results are shown by solid circles; a fit to the numerical data (not shown) gives $\Pi_n \propto U_{\rm D}^{-1.04(1)}$, in good agreement with the experimental data.

The so-called zeroth law of turbulence, first formulated in the context of classical incompressible fluids, stipulates that for fixed forcing the steady-state rate of energy dissipation tends to a nonzero constant as the viscosity vanishes ($\nu \to 0$) (*5, 33*). In our case, this corresponds to keeping F_0 fixed and taking $k_{\rm D} \to \infty$ (*34*). This law implies that the particle flux should vanish as $\Pi_n \sim k_{\rm D}^{-2}$ (see Eq. (3)), in excellent agreement with our data. Note that the steady-state energy balance also requires that $\Pi_{\mathcal{E}}$ is equal to the rate of energy input into the system, ϵ. However, energy conservation alone is not sufficient to predict the scaling of Π_n with $k_{\rm D}$, because it is not *a priori* obvious that for fixed F_0 the rate at which the system absorbs energy from the drive is not affected by changing $k_{\rm D}$ (*35*). Only *a posteriori*, from Fig. 3 (and the conservation of energy), we see that in our system the steady-state ϵ must be independent of the dissipation lengthscale down to our lowest $k_{\rm D}$. Rather remarkably, if one changed $k_{\rm D}$ dynamically, for a

system to reach a new steady state the particle flux would have to self-consistently adjust at all $k_{\rm F} < k < k_{\rm D}$, since the steady-state Π_n must be both $k_{\rm D}$-dependent (to satisfy the zeroth law) and k-independent for a given $k_{\rm D}$.

Having established a consistent picture of the steady-state fluxes in our gas, we now turn to the pre-steady-state turbulent dynamics. In Fig. 4A, we outline a consistent picture of the early-time dynamics in Fourier space. The forcing, which generates a surplus of atoms at $k_{\rm F}$, initiates the cascade at $t_{\rm s} = 0$. As the cascade front, $k_{\rm cf}(t_{\rm s})$, propagates to higher k, the steady-state momentum distribution, $n(k) \propto k^{-\gamma}$, is established in its wake (see also (*27*)). The dynamics is dissipationless until $k_{\rm cf}$ reaches $k_{\rm D}$, at time $t_{\rm d}$; only then a steady state, with matching ϵ and $\Pi_{\mathcal{E}}(k_{\rm D})$, is established. Hence, the fact that we can experimentally observe the initial dissipationless stage of turbulence ($t_{\rm s} < t_{\rm d}$), and the dependence of $t_{\rm d}$ on $U_{\rm D}$, gives us access to the dynamics of the cascade front in momentum space.

At $t_{\rm s} < t_{\rm d}$, the instantaneous particle flux is k-independent for $k < k_{\rm cf}(t_{\rm s})$, vanishes for $k > k_{\rm cf}(t_{\rm s})$, and must match the rate of the population increase in the inertial range: $n(k_{\rm cf})\, 4\pi k_{\rm cf}^2\, {\rm d}k_{\rm cf} = \Pi_n(k_{\rm cf})\, {\rm d}t_{\rm s}$, so $k_{\rm cf}^{2-\gamma}\, {\rm d}k_{\rm cf} \propto \Pi_n(k_{\rm cf})\, {\rm d}t_{\rm s}$. Analogously, for the increase of total energy in the inertial range, $k_{\rm cf}^{4-\gamma}{\rm d}k_{\rm cf} \propto \Pi_{\mathcal{E}}(k_{\rm cf})\, {\rm d}t_{\rm s}$, and $\Pi_{\mathcal{E}}(k_{\rm cf})$ is equal to the instantaneous energy-injection rate ϵ.

Assuming that ϵ, which we found not to depend on $k_{\rm D}$ in steady state, is also independent of $k_{\rm cf}$ at $t_{\rm s} < t_{\rm d}$, we get that the instantaneous $\Pi_n(t_{\rm s})$, at $k < k_{\rm cf}(t_{\rm s})$, is $\propto k_{\rm cf}^{-2}$. This gives an elegant unifying picture of the particle fluxes for $t_{\rm s} < t_{\rm d}$ and $t_{\rm s} > t_{\rm d}$ (see the inset of Fig. 4A and also (*27*)): Π_n is always the same function of the highest k for which the steady-state $n(k)$ has been established (*i.e.* the lowest k from which there is no back-flow), whether that is the instantaneous $k_{\rm cf} < k_{\rm D}$ (for $t_{\rm s} < t_{\rm d}$) or $k_{\rm D}$. This self-consistent picture also leads to a quantitative prediction that is verifiable in our experiments: the time independence of ϵ implies $k_{\rm cf}^{4-\gamma}{\rm d}k_{\rm cf} \propto {\rm d}t_{\rm s}$, which for $\gamma < 5$ and $k_{\rm D} \gg k_{\rm F}$ gives a power-law prediction $t_{\rm d} \propto U_{\rm D}^{\beta}$, with

$\beta = (5-\gamma)/2$. Specifically, for our $\gamma = 3.5(1)$ (*9*), we predict $\beta = 0.75(5)$.

In Fig. 4B, we show the variation of t_{d} with U_{D}. We find that our data is indeed well described by a power-law, with $\beta = 0.73(6)$, in agreement with our prediction. We again also show the results of our numerical simulations (solid circles), which show similar behavior with a small systematic offset; a fit to the numerical data (not shown) gives $\beta = 0.71(1)$.

Finally, it is interesting to note that the criterion for t_{d} to show scaling behavior, namely $\gamma < 5$ and hence $\beta > 0$, is intimately linked to another important concept in the theory of turbulence. For $\gamma < 5$ the steady-state spectrum has infinite energy capacity, meaning that it carries infinite energy for $k_{\mathrm{D}} \to \infty$. It is indeed generally expected for infinite-capacity systems that the cascade front propagates at a finite speed and that the Kolmogorov-Zakharov turbulence spectrum forms behind it (*36*).

Our work establishes a qualitatively new view on wave turbulence, providing a complete consistent picture of the dynamics at both short (pre-steady-state) and long (steady-state) times. In the broader context of far-from-equilibrium many-body quantum systems, a turbulent quantum gas with a large k_{D} provides a particularly interesting example of an essentially stationary non-thermal state (*37–39*). The possibility of synthetic dissipation also opens new theoretical perspectives. In the future it would be interesting to engineer arbitrary momentum-cutoff landscapes, which could, for example, allow studies of anisotropic turbulence. By dynamically tuning the dissipation scale, or the driving force, it should also be possible to study quenches between different turbulent states.

References

1. A. N. Kolmogorov, *Dokl. Akad. Nauk SSSR* **30**, 229 (1941).

2. A. Obukhov, *Dokl. Akad. Nauk SSSR* **32**, 22 (1941).

3. V. E. Zakharov, V. S. L'vov, G. Falkovich, *Kolmogorov spectra of turbulence* (Springer, Berlin, 1992).

4. S. Dyachenko, A. Newell, A. Pushkarev, V. Zakharov, *Physica D* **57**, 96 (1992).

5. U. Frisch, *Turbulence: the legacy of A.N. Kolmogorov* (Cambridge University Press, 1995).

6. O. Alexandrova, *et al.*, *Phys. Rev. Lett.* **103**, 165003 (2009).

7. J. Salort, *et al.*, *Phys. Fluids* **22**, 125102 (2010).

8. A. Chepurnov, B. Burkhart, A. Lazarian, S. Stanimirovic, *Astro. J.* **810**, 33 (2015).

9. N. Navon, A. L. Gaunt, R. P. Smith, Z. Hadzibabic, *Nature* **539**, 72 (2016).

10. W. D. McComb, *Homogeneous, isotropic turbulence: phenomenology, renormalization and statistical closures*, vol. 162 (Oxford University Press, 2014).

11. M. S. Uberoi, *Phys. Fluids* **6**, 1048 (1963).

12. M. Miyake, M. Donelan, Y. Mitsuta, *J. Geophys. Res.* **75**, 4506 (1970).

13. L. Deike, M. Berhanu, E. Falcon, *Phys. Rev. E* **89**, 023003 (2014).

14. E. A. L. Henn, J. A. Seman, G. Roati, K. M. F. Magalhães, V. S. Bagnato, *Phys. Rev. Lett.* **103**, 045301 (2009).

15. T. W. Neely, *et al.*, *Phys. Rev. Lett.* **111**, 235301 (2013).

16. W. J. Kwon, G. Moon, J. Choi, S. W. Seo, Y. Shin, *Phys. Rev. A* **90**, 063627 (2014).

17. M. C. Tsatsos, *et al.*, *Phys. Rep.* **622**, 1 (2016).

18. W. J. Kwon, J. H. Kim, S. W. Seo, Y.-I. Shin, *Phys. Rev. Lett.* **117**, 245301 (2016).

19. S. W. Seo, B. Ko, J. H. Kim, Y.-I. Shin, *Sci. Rep.* **7**, 4587 (2017).

20. M. E. Mossman, M. A. Hoefer, K. Julien, P. G. Kevrekidis, P. Engels, *Nat. Commun.* **9**, 4665 (2018).

21. S. P. Johnstone, *et al.*, *arXiv:1801.06952* (2018).

22. G. Gauthier, *et al.*, *arXiv:1801.06951* (2018).

23. B. V Svistunov, *J. Mosc. Phys. Soc.* **1**, 373 (1991).

24. D. V Semikoz, I. I Tkachev, *Phys. Rev. Lett.* **74**, 3093 (1995).

25. D. V Semikoz, I. I Tkachev, *Phys. Rev. D* **55**, 489 (1997).

26. A. L. Gaunt, T. F. Schmidutz, I. Gotlibovych, R. P. Smith, Z. Hadzibabic, *Phys. Rev. Lett.* **110**, 200406 (2013).

27. See Supplementary Material.

28. The exponent $\gamma \approx 3.5$ is close to the Kolmogorov-Zakharov prediction for (compressible) weak-wave turbulence in three dimensions, $\gamma = 3$, and in agreement with numerical simulations of the Gross-Pitaevskii equation (*9*), as well as with a scaling analysis of kinetic equations (*29*).

29. I. Chantesana, A. P. Orioli, T. Gasenzer, *arXiv:1801.09490* (2018).

30. O. Cadot, Y. Couder, A. Daerr, S. Douady, A. Tsinober, *Phys. Rev. E* **56**, 427 (1997).

31. Note that the lowest $U_{\rm D}$ we explore corresponds to $U_{\rm D}/\mu \approx 10$, $U_{\rm D}/(F_0 L) \approx 8$ and $k_{\rm D}/k_{\rm F} \approx 23$.

32. Note that it is the total radial flux Π_n, rather than $|\mathbf{\Pi}_n|$, that is k-independent in the inertial range.

33. J. C. Vassilicos, *Ann. Rev. Fluid. Mech.* **47**, 95 (2015).

34. For incompressible flows, the Kolmogorov dissipation lengthscale, analogous to our $1/k_{\rm D}$, depends on the viscosity of the fluid (as $\propto \nu^{3/4}$).

35. In most familiar systems, like the damped harmonic oscillator, the rate at which the system absorbs energy in steady state depends on both the driving and the dissipation.

36. S. Nazarenko, *Wave turbulence* (Springer, 2011).

37. M. Prüfer, *et al.*, *Nature* **563**, 217 (2018).

38. C. Eigen, *et al.*, *Nature* **563**, 221 (2018).

39. S. Erne, *et al.*, *Nature* **563**, 225 (2018).

Acknowledgments

We thank Ehud Altman, Dan Stamper-Kurn, Frédéric Chevy, and Jake Glidden for discussions, and Timon Hilker for comments on the manuscript. This work was supported by EPSRC [Grants No. EP/N011759/1 and No. EP/P009565/1], ERC (QBox), QuantERA (NAQUAS, EPSRC Grant No. EP/R043396/1), AFOSR, and ARO. N. N. acknowledges support from Trinity College (Cambridge) and the David and Lucile Packard Foundation. R. L. acknowledges support from the E.U. Marie-Curie program [Grant No. MSCA-IF-2015 704832] and Churchill College, Cambridge. R. P. S. acknowledges support from the Royal Society. K.F. was supported by JSPS KAKENHI Grant No. JP16J01683. M. T. acknowledges support from JSPS KAKENHI Grant No. 17K05548 and MEXT KAKENHI Grant No. 16H00807.

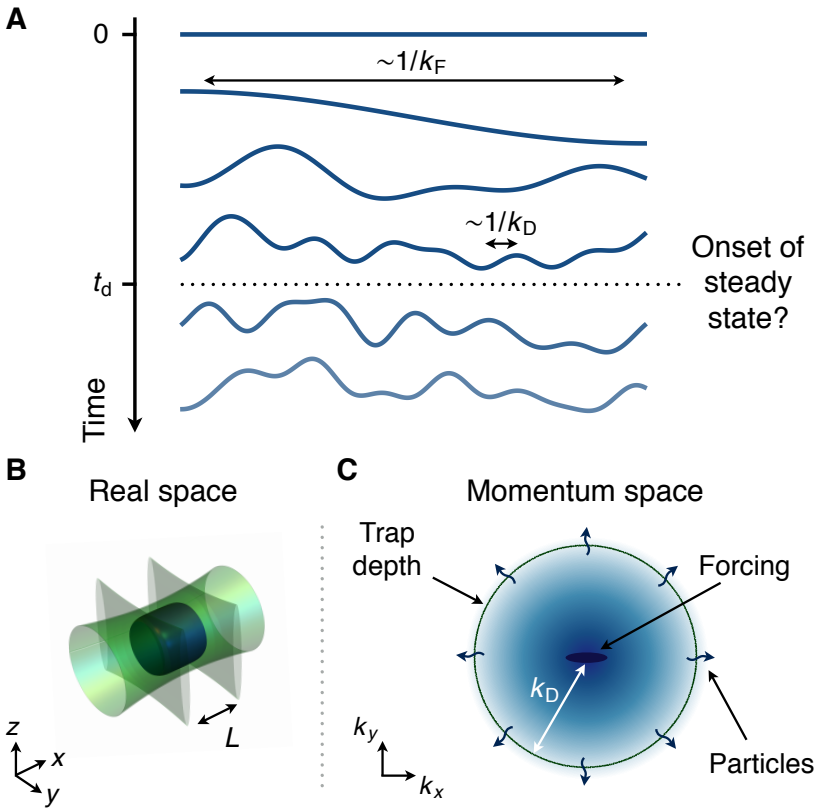

Figure 1: **Turbulent cascade in a box-trapped quantum gas.** (**A**) Cartoon of real-space dynamics of a turbulent wave. Energy is injected by forcing the matter-wave field at a large lengthscale, $1/k_{\mathrm{F}}$, and propagates to smaller scales due to nonlinear interactions. A steady state can be established once the excitations first reach the small dissipation lengthscale, $1/k_{\mathrm{D}}$, at a time t_{d}. (**B**) Sketch of the experimental setting. The atoms (blue) are trapped in a finite-depth potential formed by laser barriers (green) in the shape of a cylindrical box. The shaking force is applied along $\hat{\mathbf{x}}$. (**C**) In momentum space, the dissipation scale k_{D} is set by the trap depth; when excitations propagate to k_{D}, dissipation occurs in the form of particle loss.

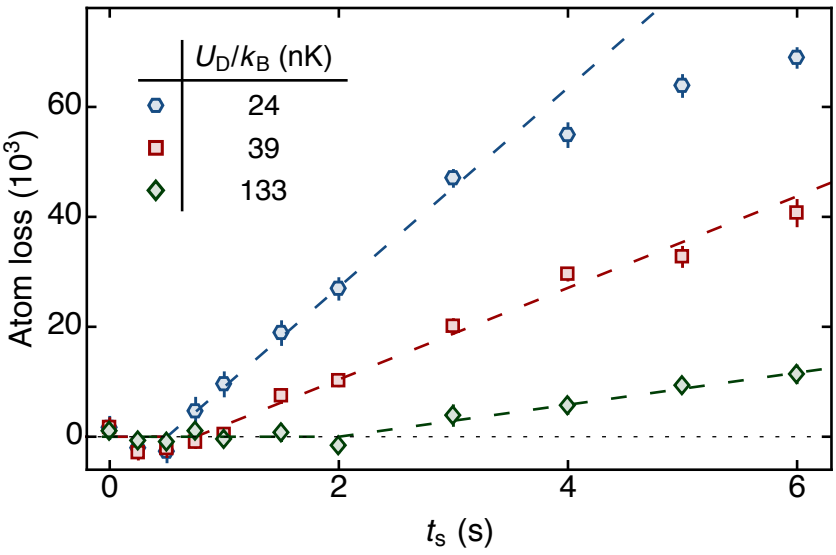

Figure 2: **Atom-loss dynamics due to the turbulent cascade.** Atoms lost versus shaking time t_s for different trap depths U_D (at $t_s = 0$ the atom number is $N \approx 1.2 \times 10^5$). Data points show averages of typically 50 measurements. Dashed lines are piece-wise linear fits. The systematic uncertainty in U_D values is 20%.

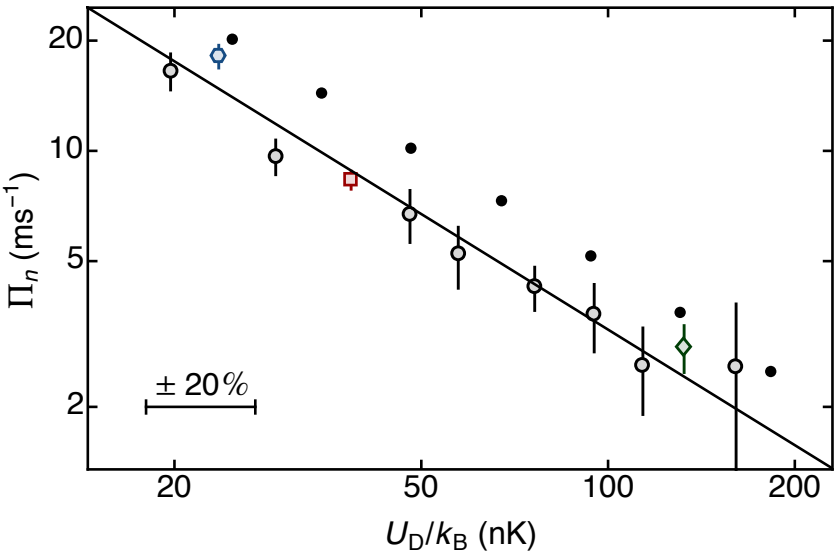

Figure 3: **Steady-state particle flux.** The atom-loss rate Π_n versus the dissipation energy scale U_D (open symbols), on a log-log plot; the three colored points correspond to the data shown in Fig. 2. Solid symbols show the results of numerical simulations. The horizontal bar indicates the systematic uncertainty in the experimental U_D values. A power-law fit to the experimental data (solid line) gives $\Pi_n \propto U_D^{-1.05(8)} \propto k_D^{-2.10(16)}$, in agreement with the theoretical prediction.

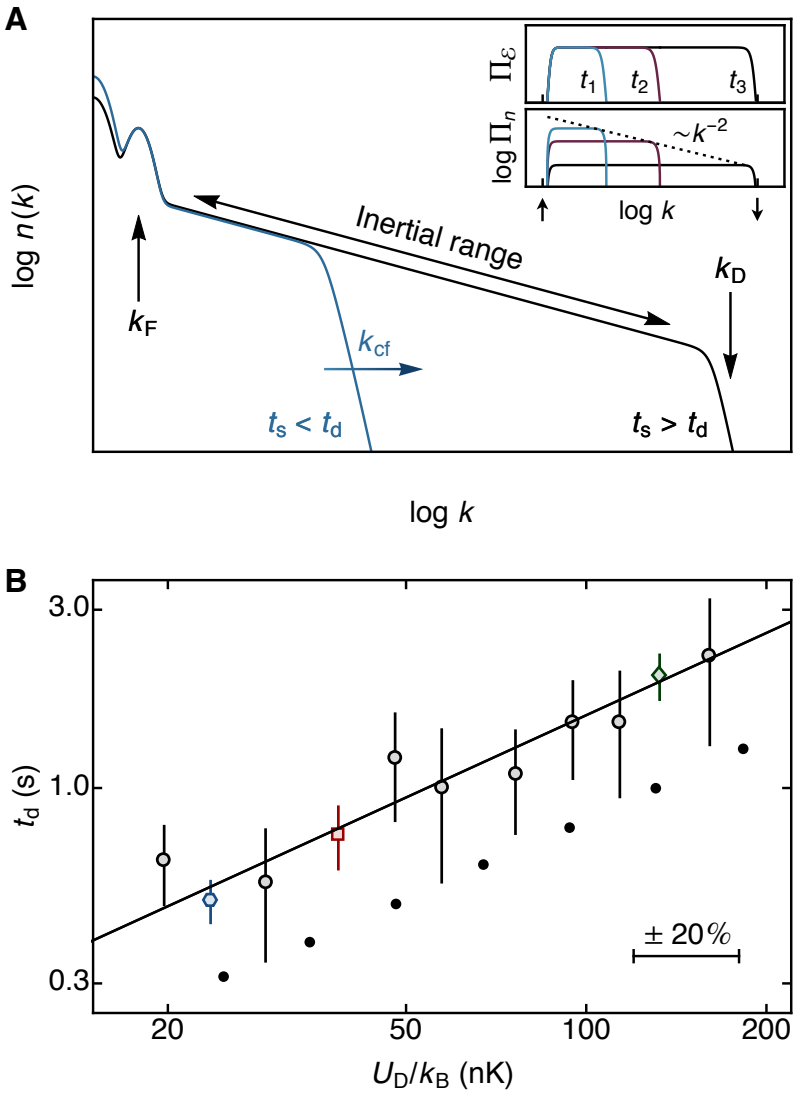

Figure 4: **Establishing the steady state: the cascade-front dynamics.** (**A**) Momentum-space turbulent dynamics. Forcing occurs at k_{F} and the steady-state distribution $n(k)$ is established in the wake of the cascade front $k_{\mathrm{cf}}(t_{\mathrm{s}})$, which propagates outwards until it reaches k_{D} at time t_{d}. For clarity of the qualitative message, here we show an idealized sketch with a very large separation between k_{F} and k_{D}; for numerical simulations with our experimental parameters see (*27*). Inset: Consistent picture for the evolution of the energy flux $\Pi_{\mathcal{E}}$ and particle flux Π_n, for three different times t_1 (blue) $<$ t_2 (purple) $<$ t_3 (black), with $t_2 < t_{\mathrm{d}} < t_3$. The forcing and dissipation scales are indicated by the vertical arrows, as in the main panel. (**B**) Onset time for dissipation. Open symbols show the measured t_{d} values versus U_{D} on a log-log plot; the three colored points correspond to the data shown in Fig. 2. Solid symbols show the results of numerical simulations. The horizontal bar indicates the systematic uncertainty in the experimental U_{D} values. A power-law fit, $t_{\mathrm{d}} \propto U_{\mathrm{D}}^{\beta}$, to the experimental data (solid line) gives $\beta = 0.73(6)$, in agreement with the prediction $\beta = 0.75(5)$.

Supplementary Materials for

Synthetic dissipation and cascade fluxes in a turbulent quantum gas

Nir Navon, Christoph Eigen, Jinyi Zhang, Raphael Lopes, Alexander L. Gaunt, Kazuya Fujimoto, Makoto Tsubota, Robert P. Smith, and Zoran Hadzibabic

Calibration of the shaking force and the resonant driving frequency

The shaking force is produced by coils that create a magnetic field gradient. We calibrate its magnitude F (for a given voltage applied to the coils) by switching off the box trap, immediately pulsing the force for a time δt, and measuring the resulting velocity kick $\delta v = F\delta t/m$; to determine δv we measure the position of the cloud's centre of mass, x_{CoM}, after a time of flight t_{ToF}.

Due to the optical resolution of the system used to create the box trap, the trap walls are not perfectly sharp [1], and consequently the frequency of the lowest axial sound mode, ω_{res}, slightly depends on U_{D}. To ensure that the gas is always driven on resonance, we measure $\omega_{\mathrm{res}}(U_{\mathrm{D}})$. We perform stroboscopic modulation spectroscopy by applying the driving force $F_0 \sin(\omega_{\mathrm{s}} t)$ for $t_{\mathrm{s}} = 2$ s, with $F_0 L \approx k_{\mathrm{B}} \times 2.5$ nK, and then releasing the cloud and measuring x_{CoM} after $t_{\mathrm{ToF}} = 140$ ms. Choosing discrete values of ω_{s} such that $\omega_{\mathrm{s}} t_{\mathrm{s}} = 2\pi j + \pi/2$, where j is an integer, the resulting x_{CoM} has an absorptive shape and we fit it with the function

$$x_{\mathrm{CoM}} \propto \frac{\omega_{\mathrm{s}}^2}{(\omega_{\mathrm{s}}^2 - \omega_{\mathrm{res}}^2)^2 + \Gamma^2 \omega_{\mathrm{s}}^2}\,, \tag{S1}$$

where Γ is the linewidth. In Fig. S1 we show such line shapes for two different U_{D}, and the plot of ω_{res} versus U_{D}.

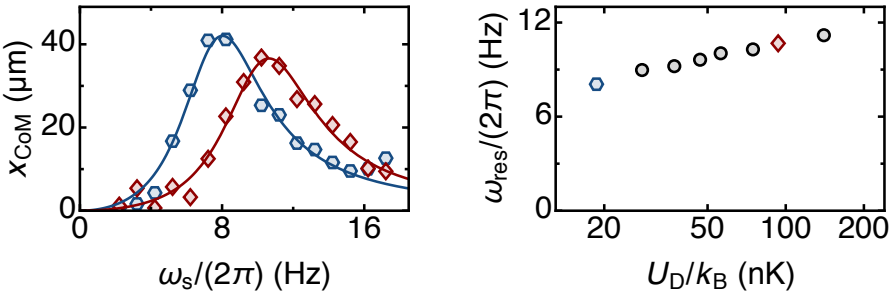

Figure S1: **The resonant drive frequency.** Left: Resonance measurements for $U_{\mathrm{D}}/k_{\mathrm{B}} = 19$ nK (blue) and 94 nK (red); solid lines are fits based on Eq. (S1). Right: ω_{res} versus U_{D}.

Numerical simulations

Gross-Pitaevskii simulations with dissipation

The starting point for our simulations is the Gross-Pitaevskii equation (GPE) for the classical field $\psi(\mathbf{r}, t)$:

$$i\hbar \frac{\partial \psi}{\partial t} = \left(-\frac{\hbar^2}{2m}\nabla^2 + V(\mathbf{r}, t) + g|\psi|^2 \right) \psi\,, \tag{S2}$$

where $g = 4\pi\hbar^2 a_s/m$ and a_s is the s-wave scattering length. If $V(\mathbf{r}, t) \in \mathbb{R}$, the evolution of the GPE conserves the total particle number $N = \int |\psi|^2 \, \mathrm{d}\mathbf{r}$. Introducing dissipation in the GPE is a subtle problem [2, 3, 4, 5]. We introduce a phenomenological term in $V(\mathbf{r}, t)$ that closely resembles the dissipation process in our experiment. We write:

$$V(\mathbf{r}, t) = V_{\mathrm{box}}(\mathbf{r}) + V_{\mathrm{osc}}(\mathbf{r}, t) - iV_{\mathrm{diss}}(\mathbf{r}),$$

where V_{box} is the box potential, V_{osc} is the forcing potential, and iV_{diss} is an imaginary 'sponge' potential that 'absorbs' particles with sufficiently high energy to leave the trap and removes them from the system. More precisely:

$$V_{\mathrm{box}}(\mathbf{r}) = \begin{cases} 0 & \text{if } |x| \leq \frac{L}{2}, \sqrt{y^2 + z^2} \leq R \\ U_{\mathrm{D}} & \text{otherwise}\,, \end{cases}$$

$$V_{\mathrm{osc}}(\mathbf{r}, t) = Fx \sin(\omega_{\mathrm{res}} t)\,,$$

and

$$V_{\mathrm{diss}}(\mathbf{r}) = \begin{cases} 0 & \text{if } |x| \leq \frac{L+2\delta}{2}, \sqrt{y^2 + z^2} \leq R + \delta \\ V_{\mathrm{D}} & \text{otherwise}\,. \end{cases}$$

The phenomenological parameter δ, the spatial offset between the edge of the box and the sponge, is introduced because even if all particles are trapped, for a non-infinite U_{D} an evanescent component of $\psi(\mathbf{r}, t)$ exists outside the box. We have verified that for a wide range of V_{D} and δ our results do not depend on their exact values (see Fig. S2 below).

We numerically solve Eq. (S2) using a pseudo-spectral method with the fourth-order Runge-Kutta time evolution. In simulations $L = 27$ μm, $R = 16$ μm, and the initial atom number is $N_0 = 1.2 \times 10^5$, corresponding to chemical potential $\mu = gn_0 = k_{\mathrm{B}} \times 2.0$ nK, where $n_0 = N_0/(\pi R^2 L)$. The size of our whole numerical grid is $40\,\xi \times 40\,\xi \times 40\,\xi$, where $\xi = \hbar/\sqrt{2mgn_0} = 1.2$ μm is the healing length. The spatial and temporal resolutions are $\frac{40}{128}\xi$ and $10^{-3}\hbar/\mu = 3.7$ μs respectively.

The initial $\psi(\mathbf{r}, t = 0)$ is determined by calculating the ground state in the static trap ($F = 0$ and $V_{\mathrm{D}} = 0$), using imaginary-time evolution of the GPE. The resonant driving frequency ω_{res} is then determined by numerically solving the Bogoliubov equations on $\psi(\mathbf{r}, 0)$. For all experimentally explored U_{D} we get $\omega_{\mathrm{res}} \approx 2\pi \times 8.8$ Hz, with variations of $< 3\%$. Finally, to simulate the shaking experiments, we solve the real-time GPE with the forcing amplitude $F = F_0 = 1.22\ \mu/L$ and nonzero V_{D}. Our results are based on a single run using the same deterministic initial condition $\psi(\mathbf{r}, 0)$.

Atom-loss dynamics

In Fig. S2 we show simulated atom loss $N_0 - N(t_{\mathrm{s}})$, where $N(t_{\mathrm{s}}) = \int |\psi(\mathbf{r}, t_{\mathrm{s}})|^2 \, \mathrm{d}\mathbf{r}$, for $U_{\mathrm{D}} = k_{\mathrm{B}} \times 25$ nK and various combinations of the dissipation parameters V_{D} and δ. In all cases we see curves similar to the experimental

ones shown in Fig. 2 in the main paper (and for the results shown in the main paper we analyze them in the same way as the experimental data). For a fixed $V_{\rm D} = 5\mu$, we get essentially indistinguishable results for any $\delta \gtrsim 7/k_{\rm D}$. Qualitatively, δ needs to be sufficiently larger than $1/k_{\rm D}$ for the probability of absorbing (on a timescale $t_{\rm s}$) particles with energies below $U_{\rm D}$ to be vanishingly small; otherwise we remove too many particles. For a fixed $\delta = 10.5/k_{\rm D}$ we get essentially the same results for any $V_{\rm D} \gtrsim \mu$.

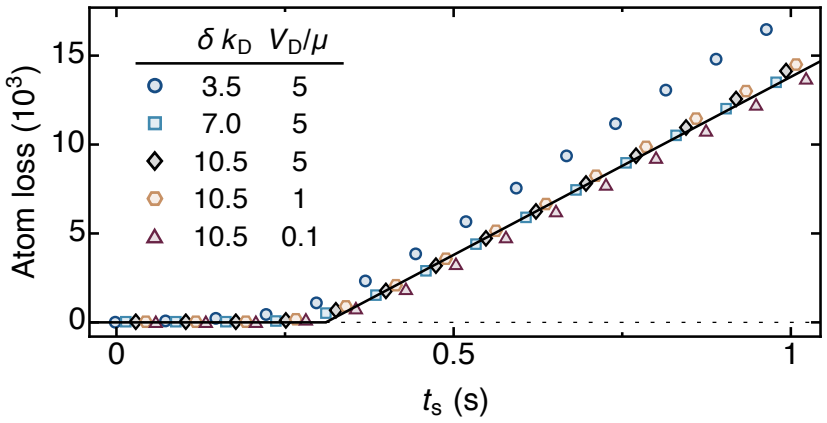

Figure S2: **Atom-loss dynamics in numerical simulations.** Atoms lost versus shaking time for $U_{\rm D} = k_{\rm B} \times 25$ nK and various combinations of the dissipation parameters $V_{\rm D}$ and δ. The solid black line is a piece-wise linear fit to the numerical data for $\delta = 10.5/k_{\rm D}$ and $V_{\rm D} = 5\mu$, from which t_d and Π_n are extracted (see main text). For clarity only a subset of $t_{\rm s}$ values are plotted.

Fourier-space dynamics

We also compute the evolution of the momentum distribution in the presence of shaking and dissipation, supporting the qualitative picture outlined in Fig. 4A in the main paper. The momentum distributions are averaged over spherical shells to obtain $n(k)$, and normalised such that $\sum_k 4\pi k^2 n(k)\delta k = N$, where $\delta k = \frac{\pi}{20\xi}$ is the grid resolution in $\mathbf{k}$ space. In Fig. S3A, we show $n(k)$ for $U_{\rm D} = k_{\rm B} \times 130$ nK and various shaking times $t_{\rm s}$. The power-law distribution $n(k) \sim k^{-\gamma}$ (with $\gamma \approx 3.5$) develops in the wake of the cascade front, and as the cascade front propagates with $k_{\rm cf}(t_{\rm s}) \propto t_{\rm s}^{1/(2\beta)}$ the momentum distribution $n(k)$ evolves in a self-similar way. As shown in Fig. S3B, this self-similarity is revealed by the collapse of the curves shown in Fig. S3A for $t \lesssim t_{\rm d}$ when plotting $n(k, t_{\rm s})$ in the rescaled form $(t_{\rm s}/t_{\rm ref})^a n((t_{\rm s}/t_{\rm ref})^{-b}k, t_{\rm s})$, with $b = 1/(2\beta) = 1/(5-\gamma) = 0.67$, $a = b\gamma = 2.33$, and setting arbitrarily $t_{\rm ref} = 1$s. Note that the successful collapse of the curves for these values of a and b also confirms our assumption that the energy input rate is time independent. Once the cascade front reaches the dissipation scale $k_{\rm D}$ (for $t_{\rm s} > t_{\rm d}$) a steady state is established over the entire inertial range.

References and Notes

[1] A. L. Gaunt, T. F. Schmidutz, I. Gotlibovych, R. P. Smith, Z. Hadzibabic, *Phys. Rev. Lett.* **110**, 200406 (2013).

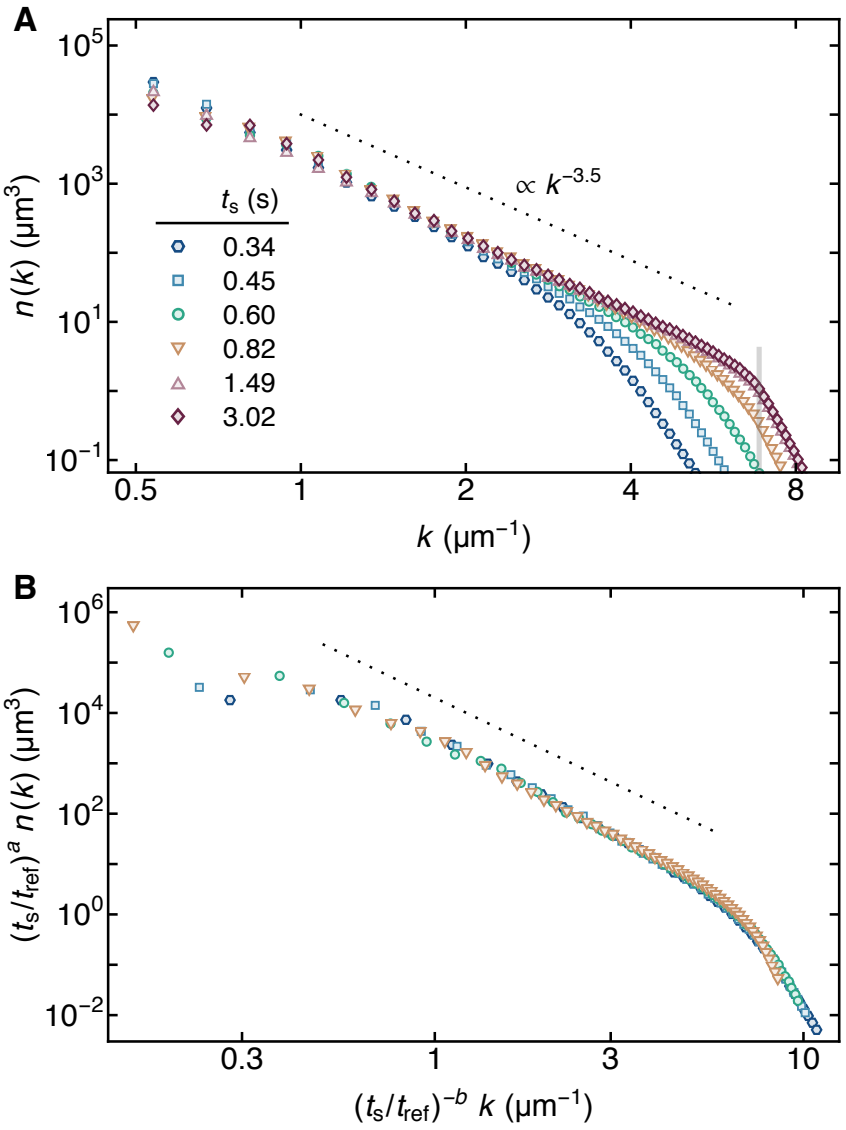

Figure S3: **Momentum-space dynamics in numerical simulations.** (**A**) $n(k)$ computed for $U_D = k_B \times 130$ nK and various shaking times t_s. The power-law momentum distribution $n(k) \sim k^{-\gamma}$, with $\gamma \approx 3.5$, develops in the wake of the cascade front. A steady state is established once the cascade front reaches k_D; in this example $k_D = 8/\xi$, indicated by the vertical grey band. (**B**) The momentum distributions from (**A**) with $t_s \lesssim t_d \approx 1.0$ s rescaled with $a = \gamma/(5-\gamma) = 2.33$, $b = 1/(5-\gamma) = 0.67$, and $t_{ref} = 1$s (see text) collapse onto a single curve, indicating self-similar behavior.

[2] M. Kobayashi, M. Tsubota, *Phys. Rev. Lett.* **94**, 065302 (2005).

[3] A. Griffin, T. Nikuni, E. Zaremba, *Bose-condensed gases at finite temperatures* (Cambridge University Press, 2009).

[4] D. Proment, S. Nazarenko, M. Onorato, *Phys. Rev. A* **80**, 051603 (2009).

[5] M. T. Reeves, T. P. Billam, B. P. Anderson, A. S. Bradley, *Phys. Rev. Lett.* **114**, 155302 (2015).